6646 *Macromolecules* **2010**, *43*, 6646–6654
DOI: 10.1021/ma1006667

Macromolecules
ARTICLE

# Smectic Demixing in the Phase Behavior and Self-Assembly of a Hydrogen-Bonded Polymer with Mesogenic Side Chains

**Manesh Gopinadhan,[†] Evan S. Beach,[‡] Paul T. Anastas,[‡] and Chinedum O. Osuji***

[†]*Department of Chemical Engineering, and* [‡]*Department of Chemistry, Yale University, New Haven, Connecticut 06520*

*Received March 28, 2010; Revised Manuscript Received July 11, 2010*

ABSTRACT: We present a detailed study of the structure and properties of a supramolecular complex formed via hydrogen bond association between poly(acrylic acid) chains and an imidazole-terminated biphenyl mesogen. The system exhibits a rich phase behavior as a function of temperature and stoichiometry, expressed as the molar ratio $S$ between the number of mesogens and binding sites present. Smectic mesophases are formed for all $S \geq 0.033$, a surprisingly small number. The dependence of the characteristic length scale of the mesophase on stoichiometry does not follow the expected 1-D swelling law. At low stoichiometries, $S \leq 0.2$, the system exhibits little or no change in structure up to temperatures as high as 200 °C, beyond which changes become temperature irreversible. In contrast, at higher $S$, the system features complex thermally driven transitions among tilted monolayer and bilayer arrangements and complete, reversible isotropization of the system at elevated temperatures. Over a limited range of temperatures and compositions, a supramolecular length scale emerges that is well beyond the upper limit imposed by a bilayer construct and thus cannot be accounted for within the conventional paradigm. Binding isotherms reveal that the polymer has a limited capacity for the ligand with saturation occurring for $S \geq 0.33$. These results suggest that the common assumption of homogeneously distributed tightly bound ligands with layer-like phase separation from the polymer backbone do not apply in this system over all compositions. The anomalous phase display is consistent with demixing between polymer rich and polymer poor domains due to the presence of excess unassociated mesogen, which can act as a solvent for the system.

## Introduction

Specific interactions between functionalized small molecules and polymer chains bearing complementary binding sites can be used to engineer supramolecular complexes that display mesomorphic structure. The use of noncovalent interactions to bind small molecules to homopolymer and block copolymer backbones is well-documented in the literature.[1−11] In particular, hydrogen-bonding interactions offer a flexible platform for the self-assembly of graft copolymer-like structures by association of linear homopolymer chains with appropriate ligands. Such supramolecular engineering permits the facile development of new materials with a wide range of functional properties. For example, photonic band gap materials[12,13] and electrically conducting supramolecular polymers[14] have been realized, in addition to materials that display orientational switching of their microstructure in the presence of electric fields.[15] In many cases, the properties and potential utility of these systems are determined in large part by the microstructure that develops because of microphase separation between the host polymer backbone and the small molecule. A common manifestation of this, for example, is the electro-optic properties that result from the formation of liquid crystalline mesophases by the small molecules when tethered to the polymer chains.[16,17]

The prototypical preparation of these materials involves complexation of the small molecule ligand to the polymer chain in solution, followed by removal of the solvent to produce a melt. The structure in the melt is considered with respect to the volume fraction of the ligand and the chemical dissimilarity between the ligand and the polymer chain, which drives phase separation. In this manner, it is very much akin to microphase separation in traditional block copolymers and comb copolymers, with the side chain motif of the comb copolymer well-reproduced by the supramolecular complex, as schematically depicted in Figure 1. The volume fraction of the ligand, $\varphi$, may be expressed in terms of the molar mass ratio, $R_M$ (assuming equal densities), between the ligand and the monomeric binding site, and the stoichiometry of the system, $S$, which is the number of ligands present per site, is shown in eq 1. In the microphase-separated state, the characteristic length scale of the system is commonly dictated by a simple 1-D swelling law.[2] As shown in Figure 1, the ligands can be organized into monolayer- (or bilayer-) type domains with dimensions set by the length of the ligand, $l$, and the tilt angle in the system, $\theta$. The repeat distance is a simple function of the layer dimensions and the volume fraction of the ligand in the system (eq 4). Finally, within the domains, the ligands may exhibit crystalline, liquid crystalline, or liquid order as a function of temperature and stoichiometry.

$$\varphi = \frac{SR_M}{SR_M + 1} \tag{1}$$

$$\varphi = \frac{t_l}{t_p + t_l} \tag{2}$$

$$d = t_p + t_l = t_p + l \sin\theta \tag{3}$$

$$d = \frac{l \sin\theta}{\varphi_l} \tag{4}$$

Implicit in this treatment is the assumption that the ligand binds stoichiometrically to the polymer backbone for all $S \leq 1$

*Corresponding authors. E-mail: chinedum.osuji@yale.edu.

 Published on Web 07/28/2010 

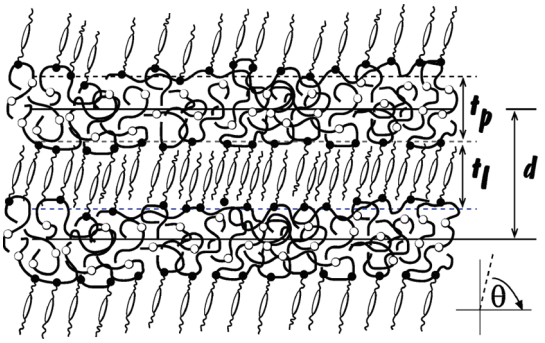


**Figure 1.** Schematic representation of one-dimensionally swelled layered structures in a hydrogen-bonded side chain of the polymer−mesogen complex. Mesogens can reversibly interact with different binding sites along the chain. The periodicity of the system is given by $d = t_p + t_l$, where $t_p$ is the thickness of the polymer layer and $t_l$ is the thickness of the mesogen layer, which takes into consideration the possible tilt ($\theta$) of the constituents.

and the supramolecular complex displays properties typical of a side-chain-functionalized polymer. Several reports in the literature have also considered supramolecular complexes at stoichiometric ratios larger than 1, with the excess ligand acting as a pseudosolvent, which can effectively swell or even dissolve the polymer.[13,18−21] Given standard concepts of polymer solution thermodynamics, it is reasonable to expect that there should be some range of composition and temperature over which the system will demix into polymer-rich and polymer-poor phases. Such demixing, together with self-assembly due to backbone−side-chain microphase separation, would make for complex phase behavior in the system. Indeed, such behavior is predicted in the specific case of weakly interacting ligands wherein the equilibrium between bound and labile species is thermally responsive at reasonable temperatures. In this situation, the quantity of solvating ligand present is strongly temperature-dependent. Such systems have been considered theoretically using the random phase approximation, in particular by Tanaka et al.[22] and Dormidontova at el.[23] In the latter study, a rich phase behavior was uncovered, marked largely by macrophase separation at elevated temperatures into ordered and homogeneous phases and additionally featuring coexistence between different ordered phases such as hexagonal and lamellar mesophases. The periodicity of ordered structures was minimized for the case of 1:1 binding and increased with positive and negative deviations from this equimolar stoichiometry. A study of the phase behavior of a poly(4-vinylphenol)-*N*,*N*-dimethyloctadecylamine system by Akiba et al. largely corroborated these findings.[20] To date, however, there are still relatively few examples in the literature of systematic studies of the phase behavior of such polymer−ligand systems where the solvency of unbound ligand plays a crucial role. Furthermore, the case of mesogenic ligands remains quite unexplored in comparison to that of flexible aliphatic ligands, such as pentadecylphenol (PDP) or dodecylbenzenesulfonic acid (DBSA), which have been more frequently considered.[2,5,24−27] Here one can expect that the ability of the ligands to form liquid crystalline mesophases could significantly impact the phase behavior of the system.

Here we report on a detailed characterization of the stoichiometry and temperature-dependent phase behavior of a supramolecular complex produced by hydrogen bonding a mesogenic imidazole-terminated ligand to a poly(acrylic acid) (PAA) backbone. The binding of the mesogen to the polymer backbone is seen to saturate for stoichiometric ratios $S \geq 0.33$. Beyond this saturation of the polymer's binding capacity, additional mesogens are successfully incorporated into the system via free association (coassembly) with bound species, resulting in

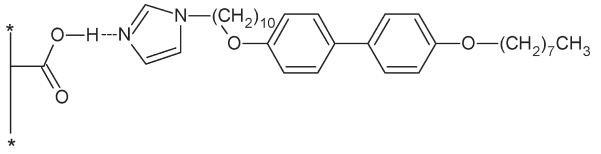


**Figure 2.** Chemical structures of the PAA homopolymer and the H-bonded imidazole mesogen.

crystallization of the mesophase at sufficiently high loading densities. We present a model wherein smectic demixing between mesogen rich and mesogen poor domains develops because of the activity of the unbound mesogen as a solvent at high temperatures. A characteristic length scale develops as macrophase separation is inhibited by the connectivity provided by the polymer backbone, which participates in both phases via hydrogen bonding with the mesogens.

## Experimental Section

**Materials and Sample Preparation.** Polydisperse atactic PAA of molecular weight 450 kg/mol. was obtained from Polysciences and used as received. The mesogenic ligand, with a molecular weight of 0.504 kg/mol, is based on an imidazole headgroup and a rigid biphenyl core with 10 and 8 carbon aliphatic spacer and tail segments, respectively as illustrated in Figure 2. The ligand was synthesized starting from 4,4′-dihydroxybiphenyl, as described in the Supporting Information. Complexes were produced over a range of stoichiometric ratios from $S = 0.011$ to 1 by combining appropriate quantities of 2.5 wt % DMF (Aldrich) solutions of the polymer and mesogen while mixing with a magnetic stirrer. DMF was removed by slow evaporation at 75 °C over several hours. The films produced were dried under vacuum at 65 °C for 48 h and then used without further treatment.

**X-ray Scattering.** Small-angle X-ray scattering (SAXS) and wide-angle X-ray scattering (WAXS) were performed on a Rigaku S-3000 system using pinhole collimation of Cu Kα radiation at 1.54 Å. SAXS patterns were recorded on a 2-D electronic wire detector (1024 × 1024 pixels), and WAXS was recorded on 20 × 25 cm image plates (Fuji). Data were analyzed using MATLAB routines (Rigaku) to integrate the 2-D data to provide 1-D representations of scattered intensity versus wavevector $q$, where $q = (4\pi/\lambda) \sin \theta$, with $2\theta$ the scattering angle. Temperature-dependent measurements were made using a hot stage (Linkam THMS600) with associated temperature controller (TMS 94). The sample chamber was evacuated and then refilled with helium to provide a low scattering atmosphere that aided heat transfer between the hot stage and the polymer films. Samples were subjected to a heating rate of 10 °C/min and allowed to equilibrate for 10 min at each temperature prior to measurement. Data were collected for 10 min at each temperature.

**Differential Scanning Calorimetry and Optical Microscopy.** Differential scanning calorimetry (DSC) was conducted on a TA Instruments Q200 using a fast heating rate of 40 °C/min and a slow heating rate of 5 °C/min. Birefringent sample textures were observed as a function of temperature by polarized optical microscopy using a Zeiss Axiovert 200 M inverted microscope. There was a constant offset of approximately 5 °C between temperatures recorded by DSC as compared with SAXS (higher).

**Fourier Transform Infrared Spectroscopy (FTIR).** Attenuated total reflectance (ATR) Fourier transform infrared spectroscopy (FTIR) measurements on melt samples were conducted with a Bruker Tensor 27 spectrometer equipped with a temperature-controlled Pike Si-crystal ATR cell. Samples were prepared by temperature-controlled solvent evaporation directly on the cell to ensure good conformal contact of the polymer film with the crystal.

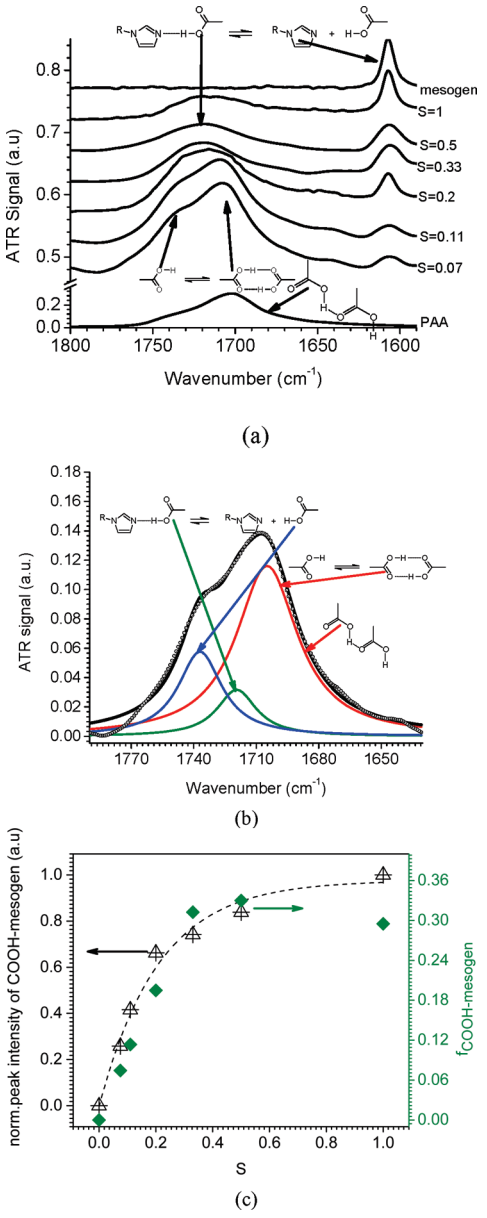


**Figure 3.** (a) IR spectra of PAA homopolymer, the imidazole mesogen, and its blends at different compositions in the carboxylic stretching region (1800−1600 $cm^{-1}$) recorded at 30 °C. (b) Illustration of the peak deconvolution procedure for complexes. The carboxylic stretching band is Lorenzian deconvoluted into three contributions: (i) the stretching band around 1737 $cm^{-1}$ corresponds to free carboxylic groups (blue line), (ii) the band around 1720 $cm^{-1}$ is due to carboxylic groups involved in the COOH−imidazole binding (green line), and (iii) band around 1703 $cm^{-1}$ is attributed to the carboxylic groups in dimerized form or due to intramolecular hydrogen bonding (red line). The circles represent the experimental data, and the solid black line represents the sum of three Lorenzian contributions. (c) The contribution from the carboxylic groups hydrogen bonded to mesogens at various blend ratios. The measured intensities at different molar ratios are scaled by taking into account the amount of PAA in the system and then normalized to the intensity at $S = 1$. It is evident that the hydrogen bonding saturates around 0.33 molar ratio. The dashed line is a sigmoidal fit to the normalized peak intensity.

## Results and Discussion

**FTIR.** Hydrogen bonding between the imidazole acceptor of the ligand and the hydroxyl donor of the polymer chain was confirmed by ATR-FTIR measurements, Figure 3a. The infrared absorption spectra were analyzed using Lorentzian deconvolution to separate the different contributions to the carboxylic band. Melt-phase PAA showed the characteristic stretching band of the carboxylic group centered around 1700 $cm^{-1}$, which was deconvoluted into two separate contributions. At room temperature, the band at 1737 $cm^{-1}$ is attributed to the free C═O stretching (COOH groups not involved in any H-bonding), whereas the band around 1703 $cm^{-1}$ is due to the combination of COOH groups that are hydrogen bonded in dimeric and intramolecular form.[28,29] The addition of the mesogen leads to the display of carboxylic stretching with frequencies centered on ∼1717−1723 $cm^{-1}$, as evident from the modification of the interaction spectrum depicted in Figure 3a. This is consistent with the formation of hydrogen bonds between imidazole and carboxylic groups and is also observed for the closely related pyridine−carboxlic acid pairing.[28,30] This was taken as the primary indicator of H-bond formation between the imidazole-terminated mesogen and the acrylic acid units of the polymer. The fraction of the imidazole-bound carboxylic groups at different temperatures is obtained by fitting the carboxylic band with a three-band model, as shown in Figure 3b. Analysis of the deconvoluted peaks at the carboxylic region permits quantification of the fraction of the carboxylic groups involved in hydrogen bonding with the imidazole headgroup of the mesogen as a function of stoichiometry at a fixed temperature. The fraction of the carboxylic groups hydrogen bonded to the mesogen, $f_{COOH-mesogen}$, can be estimated[28] using eq 5.

$$f_{\mathrm{COOH-mesogen}} = \frac{A_{\mathrm{COOH-mesogen}}/A_{\mathrm{free}}}{1+\varepsilon_1(A_{\mathrm{COOH-mesogen}}/A_{\mathrm{free}})+\varepsilon_2(A_{\mathrm{dimer/intra}}/A_{\mathrm{free}})} \quad (5)$$

Here $A_{free}$, $A_{COOH-mesogen}$, and $A_{dimer/intra}$ are the peak areas corresponding to free, hydrogen-bonded carboxylic−mesogen, and combination of dimer and intramolecular hydrogen-bonded carboxylic groups, and $\varepsilon_1$ and $\varepsilon_2$ are the respective ratios of the absorptivities. The absorptivity ratio $\varepsilon_2$ is 1.5 and $\varepsilon_1$ is taken close to unity.[31]

Peak deconvolution analysis reveals that the peak intensity contribution in arbitrary units due to COOH−imidazole binding increases with increasing stoichiometry before saturating around $S = 0.33$, as depicted in Figure 3c. This is in excellent agreement with the calculated fraction of carboxylic groups involved in hydrogen bonding with imidazole units, shown on the same plot. The implication is that for $S \geq 0.33$, all monomer units along the polymer chain are involved in hydrogen bonding, either with the imidazole mesogen or other acrylic acid groups, or they are otherwise not accessible for imidazole binding, possibly due to bulkiness and rigidity of the mesogenic groups.[32] Beyond this binding saturation limit, excess mesogens in the system simply associate loosely or coassemble with the already bound moieties because they do not macrophase separate from the polymer. Studies were also conducted as a function of temperature, but no large scale changes are observed for temperatures up to 170 °C. Figure 4 shows the fraction of mesogen-bonded COOH groups as a function of temperature for $S = 0.075$, 0.11, and 0.50. Elevated temperatures of sufficient magnitude could be expected to promote dissociation of COOH dimers as well as COOH−imidazole pairs. Heating the sample also provides mobility to the coassembled but non-hydrogen-bonded mesogens that are present in the system in excess of the binding capacity of the polymer chain for $S \geq 0.33$. These species, however, do not contribute

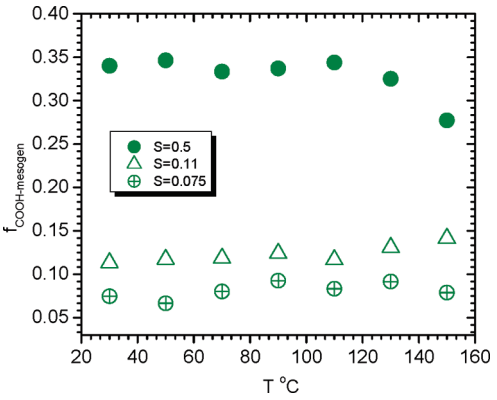


**Figure 4.** Peak fraction of COOH groups involved in hydrogen bonding with imidazole head groups for $S = 0.075$, 0.11, and 0.5 at different temperatures as indicated. For low stoichiometry complexes, the fraction of the hydrogen bonds attributable to the mesogen does not show any significant temperature dependence, whereas there is a slight decrease at elevated temperatures for $S = 0.5$.

to increased band intensity at elevated temperatures. The fact that the fraction of mesogen-bonded COOH groups does not change significantly with temperature suggests that the thermal dissociation of COOH dimers and COOH−imidazole pair occurs to roughly the same degree and does not result in any new hydrogen bond formation; if any COOH groups are liberated by thermal dimer breakage, then they do not participate in hydrogen bonding with the mobile mesogens in the system, and thus the binding saturation limit does not increase at elevated temperatures. At temperatures beyond 170 °C, the formation of acid anhydride by dehydration of neighboring COOH groups becomes non-negligible, leading to irreversible changes in the observed infrared absorptions as well as phase behavior, as studied by SAXS, DSC, and POM.

**Differential Scanning Calorimetry.** The PAA used in this study is an atactic amorphous polymer, with DSC showing a glass transition, $T_g$, at 132 °C. The mesogen is a crystalline solid at room temperature, with a single, well-defined melting point at 97 °C. DSC traces for both the polymer and mesogen are provided in the Supporting Information (Figure S1). X-ray scattering of the compacted mesogen powder shows a layered structure with a long period of 33 Å, in good agreement with the calculated extended chain length of the molecule, 34 Å. On formation of the complex, the mesogenic ligand exerts a plasticizing effect on the PAA chains, resulting in a decrease in the glass-transition temperature to roughly 60 °C (Figure 5). However, from $S = 0.011$ to 0.2, the $T_g$ does not show a composition dependence. For these samples, with the exception of the glass transition, the DSC data are remarkably featureless. Beyond $S = 0.2$, the glass transition was not observable, even at fast heating and cooling rates of 40 °C/min shown in the Supporting Information. For these samples, multiple endothermic peaks are observed on heating at temperatures between about 70 and 150 °C with a very broad final or clearing transition. For $S \geq 0.2$, the general features of system are an increasing melting enthalpy (normalized with respect to the mass content of the mesogen) on increasing stoichiometry for the first transition, around 80−95 °C, and a relatively conserved enthalpy for the second transition, located around 96−105 °C. Beyond this temperature, the remaining transitions are of marginal strength and are not well-resolved in all cases. These general features are consistent with those of prior observations involving complexes prepared using low molar mass PAA with narrow molecular weight distribution derived by anionic synthesis.[12,33] The high molecular weight and polydispersity of the PAA used in the current study likely contribute to a broadening of the transitions reported here.

The presence of transitions close to that of the neat ligand around 97 °C may lead one to conclude that there is macrophase separation in the system between the polymer and the pure crystalline mesogen. However, no evidence of the neat crystalline mesogen was found in SAXS nor in POM studies. The location of the largest exothermic peak on cooling was around 80−95 °C which is inconsistent with the crystallization of the pure mesogen. Finally, the measured DSC traces were all completely reversible, which is in contrast with those encountered for improperly prepared blends that display macroscopic regions of the pure mesogen distributed throughout the polymer film.

**Polarized Optical Microscopy.** Polarized optical microscopy shows the formation of homogeneous films over all stoichiometries. For $S \geq 0.075$, the films are birefringent and display liquid crystalline textures, as shown in Figure 6. For $S \geq 0.20$, heating to temperatures above 150−180 °C results in a loss of birefringence as the samples go though an LC-to-isotropic transition that corresponds roughly with the final weak, broad endothermic peaks observed in DSC. For $0.20 > S \geq 0.075$, birefringence was maintained without a significant decrease in the transmitted light intensity up to 200 °C. Samples heated beyond 200 °C showed a loss of birefringence that was not recovered on cooling to room temperature, likely due to anhydride formation and degradation of the polymer. The observation of mesophase formation at such low stoichiometries is quite remarkable. At $S = 0.075$, only 1 out of every 13 to 14 acrylic acid repeat units bears a ligand. Even at $S = 0.033$, where 1 in 33 units is complexed, although the samples were not birefringent, scattering studies reveal that there is a modest degree of mesoscale ordering between the ligands, as will be discussed.

**X-ray Scattering.** SAXS shows a single strong scattering peak centered around $q = 0.08-0.1$ Å$^{-1}$ for $S = 0.033$, 0.075, 0.11, and 0.20 at room temperature (Figure 7). The peak positions and intensities were found to be quite independent of temperature up to 160 °C, in agreement with the observations from polarized optical microscopy described above. The $S = 0.20$ sample also has a weak shoulder located at 0.13 Å$^{-1}$ and a smaller peak at 0.26 Å$^{-1}$. For $S \geq 0.33$, with the exception of $S = 0.50$, the system in general shows a much weaker primary peak between 0.125 and 0.175 Å$^{-1}$, with a second order present at higher $q$. For $S = 0.5$, the primary reflection was observed at $q = 0.32$ Å$^{-1}$, with a second-order reflection present at higher $q$, observed in the wide-angle regime. The variation in the $d$-spacing of the primary LC mesophase-related SAXS peak at room temperature as a function of stoichiometry is shown in Figure 8. For $S = 0.033$, 0.075, and 0.11, the mesophase displayed by the system has $d$-spacings of 67, 65, and 64 Å. Given the extended chain length of 34 Å for the ligand, one possibility is to rationalize this dimension in terms of a homogeneous distribution of ligand monolayers separated by a volume fraction proportional thickness of intervening PAA. This 1-D swelling approach, however, not only fails to predict the $d$-spacing for the system accurately, but the measured dependence of the $d$-spacing with stoichiometry also deviates from that expected based on 1-D swelling. Alternatively, we may account for the ~66 Å dimension in terms of a dense arrangement of tilted ligand bilayers. This implies that the system would be inhomogeneous in the spatial distribution of the ligand but instead displays some heterogeneity such that the mesogens are locally dense in some regions, giving rise to mesophases with layer spacings that would be

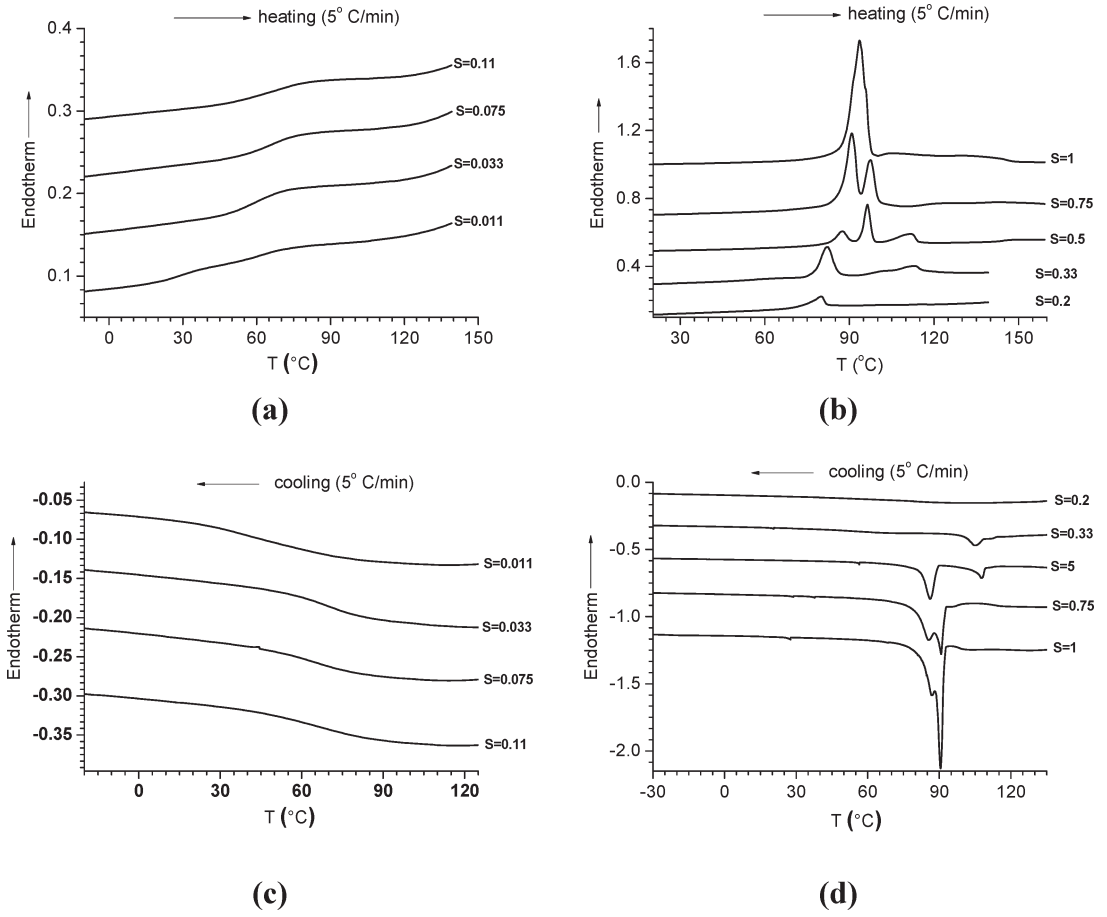


**Figure 5.** DSC heat flow curves of PAA−mesogen complexes of various stoichiometries, $S$, taken on second heating/cooling at 5 °C/min.

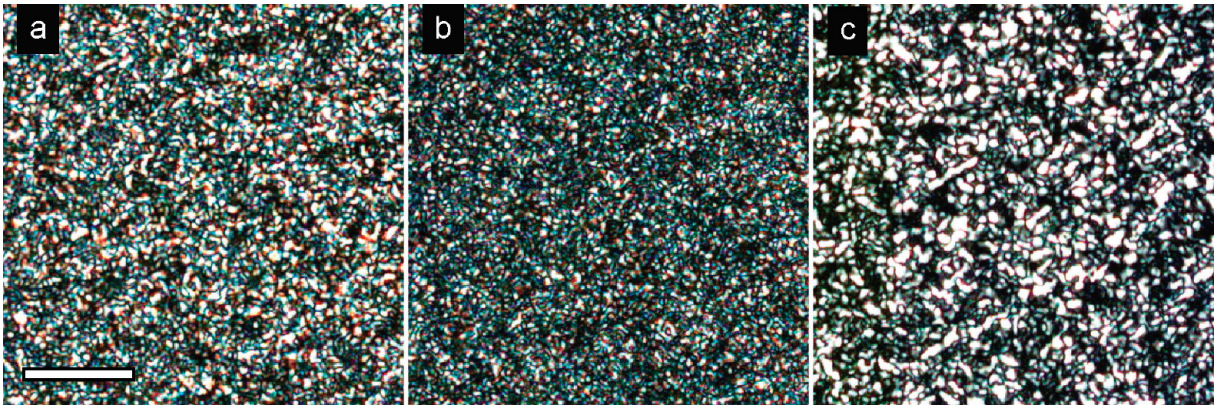


**Figure 6.** Polarized optical micrographs of PAA−mesogen complex melts. (a,b) $S = 0.5$ sample at 30 and 120 °C, respectively. At temperatures above 160 °C, the birefringence was extinguished. (c) $S = 0.11$ sample at 30 °C. The scale bar is 50 $\mu$m.

expected at higher nominal stoichiometries based on a bilayer construct. Whereas this is an intriguing possibility, our experiments did not produce robust indications of the presence of microscale heterogeneity in the system via neither optical nor scattering techniques. At this time, the reasons for the deviation from the expected swelling behavior remain unclear.

An examination of the wide-angle scattering data (Figure 9) at room temperature as a function of stoichiometry shows that for low stoichiometries, the ligands do not display strong positional correlations inside the mesophase. That is, they have liquid-like order, as illustrated by the broad diffuse scattering for $S = 0.11$. At $S = 0.2$, the mesophase starts to display some order via the development of a small peak in the scattering signal at $q = 1.455$ Å$^{-1}$, corresponding to $d = 4.3$ Å. Finally, for $S \geq 0.5$, the samples display quite strong peaks located at $q_\circ = 1.455$ and 1.653 Å$^{-1}$, corresponding to $d = 4.3$ and 3.8 Å, respectively. These peaks are due to the crystallization of the mesogen, and their positions are consistent with those observed for the pure mesogen itself. The peak at 4.3 Å is likely due to side−side correlations of the biphenyl cores, whereas that at 3.8 Å is produced by tight packing of the alkyl tails and spacers of the mesogen.

A preliminary phase diagram for the system has been constructed on the basis of SAXS, WAXS, POM, and DSC studies (Figure 10). There are likely several regimes of

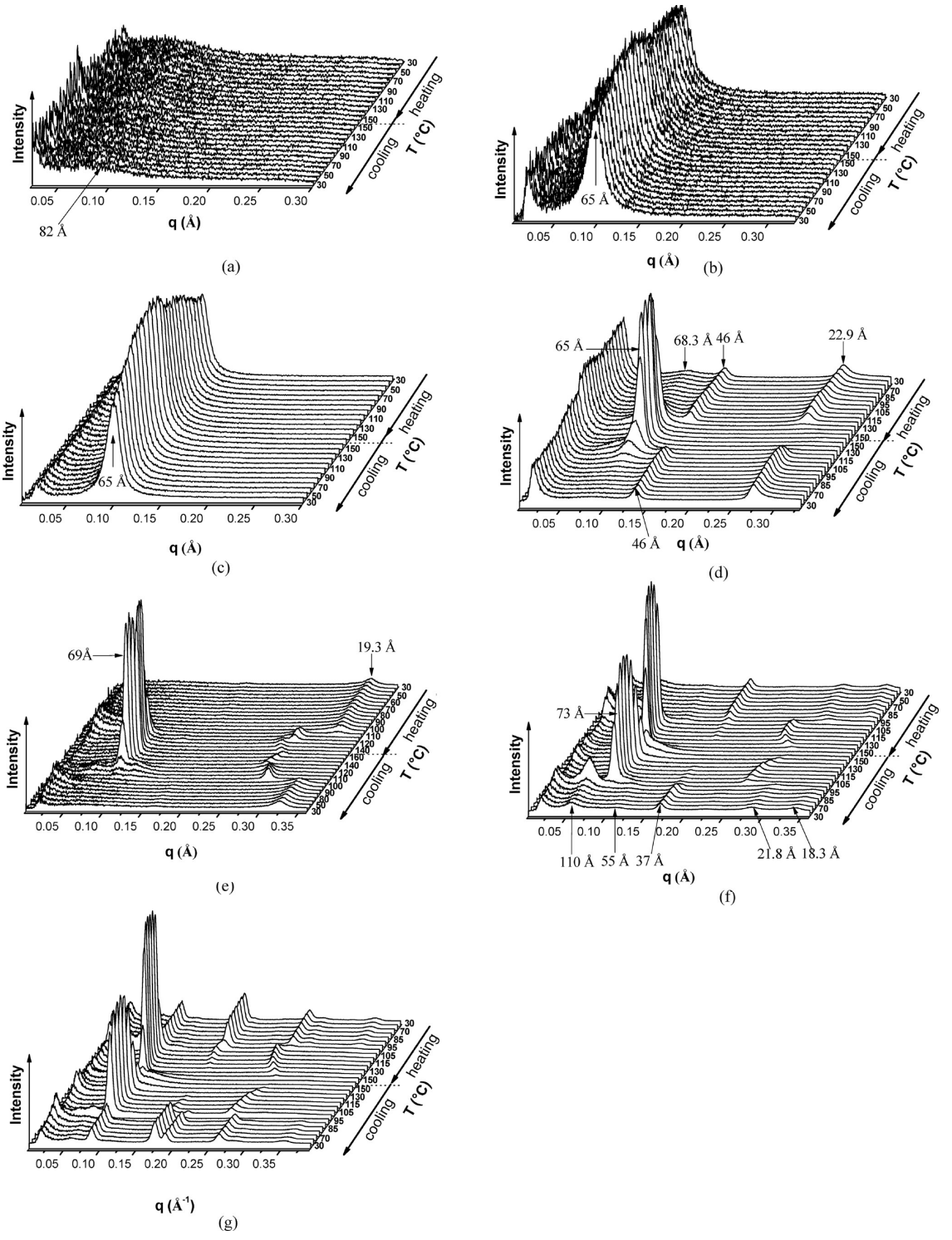


**Figure 7.** Circularly integrated SAXS data from second heating and cooling of the melt samples as a function of temperature at different stochiometries: $S$ = (a) 0.011, (b) 0.033, (c) 0.075, (d) 0.33, (e) 0.5, (f) 0.75, and (g) 1. Data for $S$ = 0.11 and 0.2 are largely identical to those for $S$ = 0.075 and are provided instead in the Supporting Information.

coexistence between different smectic mesophases, particularly at elevated temperatures, but these could not be accurately delineated here.

As seen from the data of Figure 7, higher stoichiometry systems, $S \geq 0.33$, showed a marked dependence of their structure on temperature, in contrast with lower stoichiometry samples. For $S$ = 0.50, 0.75, and 1.0, cooling from the isotropic state at elevated temperatures results in the development of a scattering peak at $d \approx 110$ Å, around $T$ = 95−110 °C. The peak is of limited intensity compared with the liquid crystalline scattering at immediately proximate temperatures, but in the case of $S$ = 1.0, for example, higher order peaks at 2q* and 3q* are shown, suggestive of a layered structure. For $S$ = 0.50, the peak persists only over a limited range of roughly 10 °C, whereas for $S$ = 0.75 and 1.0, the peak was found to persist on cooling to room temperature with relatively low intensity. From the schematic previously provided in Figure 1, it is clear that this length scale

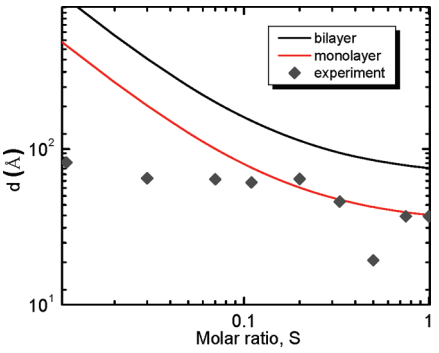


**Figure 8.** Sample periodicity as a function of stoichiometry of the complex as deduced from SAXS data is compared with 1-D swelling models based on nontilted monolayer or bilayer constructs. The long periodicity (d) of a 1-D swelled monolayer system for example is the sum of the length of the mesogen ($l$) and the thickness of the polymer layer ($t_p$), providing $d = l/\varphi = ((S \times R_M + 1)/(S \times R_M)) \times l$; $R_M$ is ratio of the molecular weight of the mesogen and that of polymer monomer, which is equal to 7 in this case.

cannot be accounted for in the conventional manner where the extended length of the side group is used as a fundamental unit, whereby the system is limited to displaying periodicities that are roughly double this dimension. This neglects any dilution of the mesogen by the presence of the polymer, which is a reasonable assumption at these high stoichiometries. Given the ratio of the molar mass of the mesogen to the acrylic acid monomer ($R_M = 7$), at $S = 0.50$, for example, the mesogen constitutes roughly 78% of the system by mass, and at $S = 1.0$, it makes up 87.5 wt % of the sample. The emergence of structure on this length scale in these systems has been reported before, for $S = 0.5$, using polymer backbones of 5 and 21 K molecular weights.[33] The observation here of the same layer-like order using a polymer backbone of significantly higher molecular weight is striking. It suggests that the system selects a length scale that is independent of the polymer chain length, in stark contrast with the common experience for block and comb copolymers where microphase separation is intrinsically related to chain dimensions. The temperature-dependent phase behavior at these high stoichiometric ratios is exceptionally complex. There appear to be multiple transitions between different structures, and clearly, there are temperatures at which some of these structures are in coexistence. Notwithstanding this complexity, however, the consistent feature is that the 110 Å structure forms during the transition from the presumed bilayer arrangement at elevated temperatures that give rise to ~66−72 Å scattering and the structures that are present at lower temperatures, ranging from 20 to 40 Å. This observation is in good agreement with previous results for this same system at $S = 0.50$.

The presence of multiple apparent LC phases during the transition from the 110 °C temperature range to room temperature provides insight into a possible mechanism to explain the appearance of the supramolecular peak at 110 Å. Taken together with the results of our FTIR measurements that conclusively show that the polymer has a limited binding capacity for the mesogen, we propose a model based on smectic demixing, as shown in Figure 11.

Here unbound mesogens are coassembled with bound species at elevated temperature, yielding a homogeneous phase with a smectic layer spacing of roughly 66−72 Å. This behavior at elevated temperatures is similar to the behavior of the system at low stoichiometries across all temperatures, where a homogeneous liquid crystalline medium is formed. On reducing temperature, the system starts to demix in the

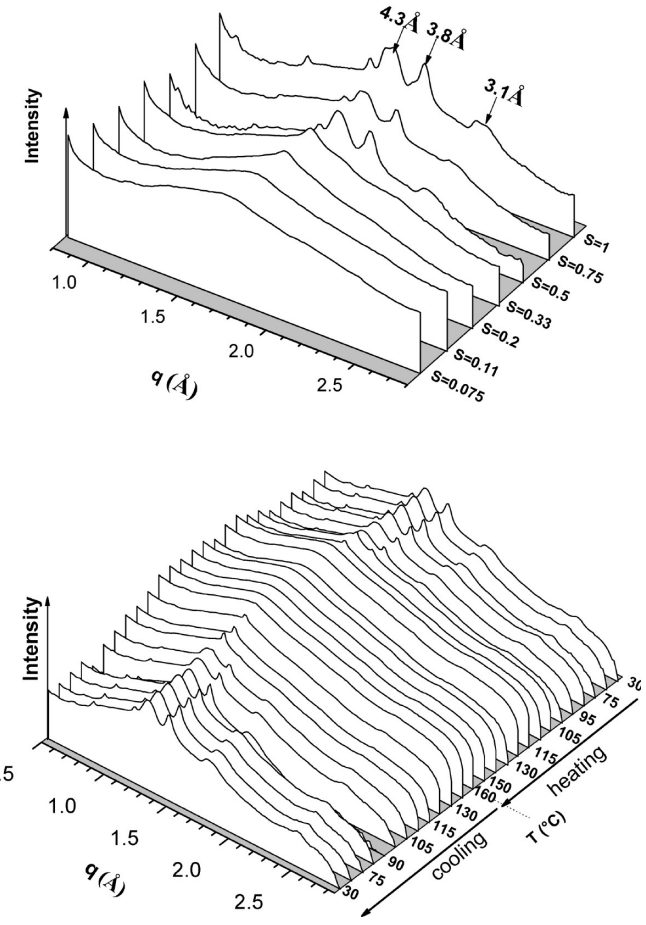


**Figure 9.** Top: WAXS data for different $S$ at 30 °C, as indicated. Bottom: WAXS data obtained during a heat−cool ramp for $S = 0.5$ at selected temperatures, as indicated.

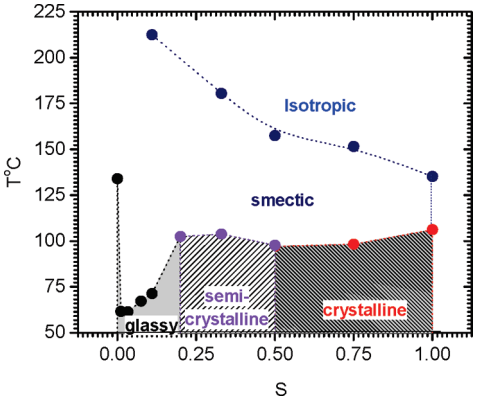


**Figure 10.** Phase diagram for the hydrogen-bonded PAA−imidazole mesogen system.

typical fashion encountered for UCST systems. Here the two components are the liquid crystalline polymer presented by the combination of the polymer with bound mesogen and the solvent composed of the mesogens in the liquid state, coassembled loosely with the bound mesogens. In this sense, this is akin to demixing between LCPs and LC solvents where nematic−isotropic, nematic−nematic, smectic−isotropic, and smectic−smectic phase coexistence can be found.[34−43] The system here demixes into mesogen-rich and mesogen-poor domains. We propose that the mesogen-poor phase possesses the same ~66−72 Å periodicity that is found in the homogeneous low stoichiometric ratio materials, whereas

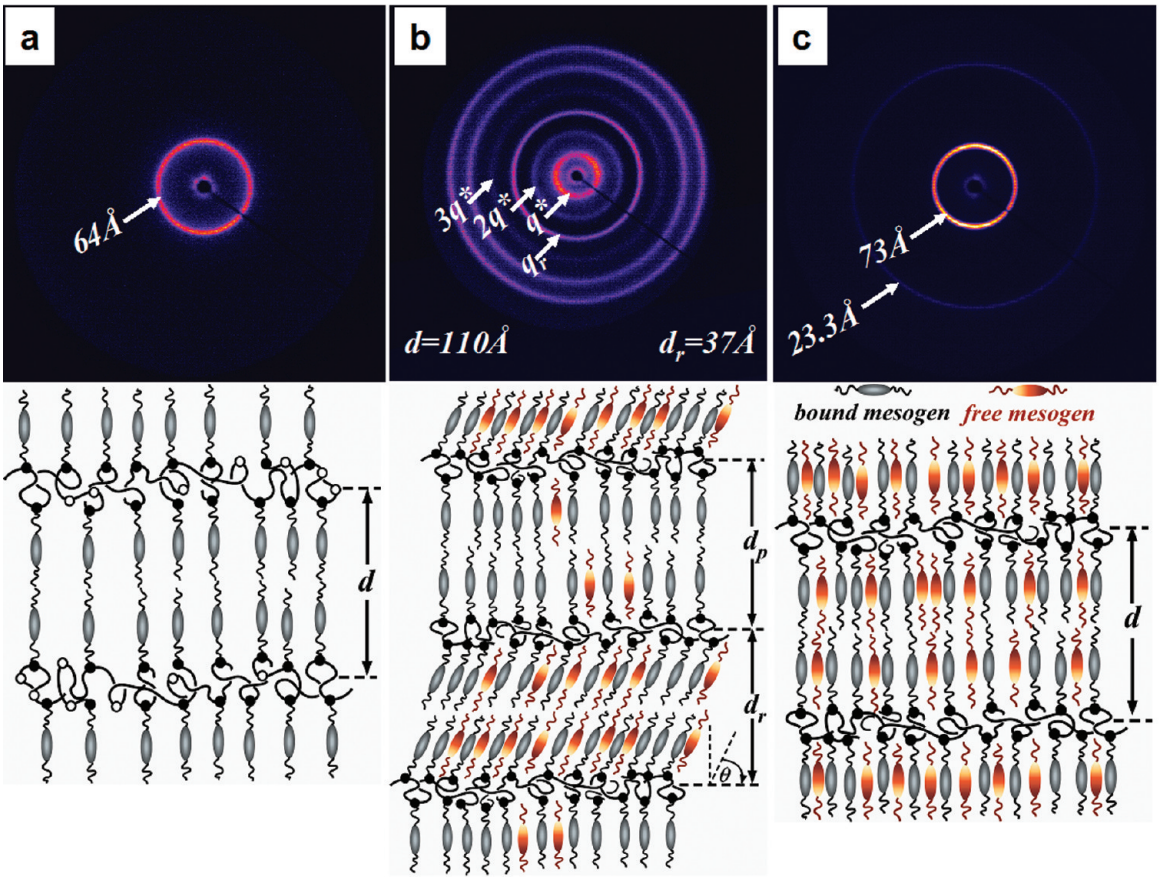


**Figure 11.** 2-D scattering patterns (top) and the corresponding schematic representations of the possible arrangements of the mesogens (bottom): (a) $S = 0.11$ recorded at 30 °C. The mesogens adopt a loosely packed bilayer structure at all temperatures with a periodicity of about twice the length of mesogen. All mesogens are bound. (b) $S = 0.75$ sample at 30 °C. The scattering due to the large length scale (~110 Å) smectic demixed structure is clearly visible out to the third-order reflection. The scattering vector at $q_r = 0.17$ Å$^{-1}$ corresponds to a periodicity of $d_r = 37$ Å that is due to a tilted bilayer packing of the mesogens, as shown in the schematic. The distinctive $d = d_r + d_P = 110$ Å length scale implies an alternating arrangement of mesogen rich ($d_r$) and mesogen poor ($d_p$) domains. (c) $S = 0.75$ at 130 °C. The system adopts a bilayer structure in which free mesogens are coassembled with hydrogen-bonded mesogens.

the mesogen-rich phase can adopt a dense tilted monolayer or interdigitated bilayer arrangement, with smectic layer spacings of roughly 37 Å. Crucially, macrophase separation here is prevented by the involvement of the PAA backbones in both the mesogen-rich and mesogen-poor domains via bound mesogens. This establishes the characteristic length scale as a simple combination of the two existing length scales in the sample (Figure 11b). Unsurprisingly, this phase separation occurs in the vicinity of the crystallization temperature of the mesogen, and it is likely that it is driven by the crystallization of mesogen-rich domains. This point is underscored by an examination of the temperature-dependent WAXS, discussed below.

In contrast with the thermal character of the pure mesogen, melting of the ordered mesophases on the 3−5 Å length scale is not a simple one-step process with a well-defined transition temperature. As seen in Figure 9, on heating the $S = 0.50$ sample from room temperature, the 3.8 Å peak disappears just above 100 °C, concomitant with a sharpening of the 4.3 Å peak. This 4.3 Å peak remains superimposed on the broad hump originating from the amorphous polymer chain. The peak gradually recedes at temperatures above about 120 °C. On cooling, it re-emerges around 120 °C, followed by the 3.8 Å peak near 105 °C. At this temperature, higher order peaks also emerge and strengthen considerably as the sample cools. We propose that the 4.3 Å peak is due to positional correlations between the biphenyl cores of the mesogens, whereas the 3.8 Å peak (and others at higher $q$) originate because of the packing of the 8 and 10 carbon long aliphatic spacer and tails of the mesogen. The broadening of the 4.3 Å peak that occurs on the development of the 3.8 Å peak and the quasi-isothermal sharpening that occurs when the 3.8 Å peak disappears on heating certainly support this view. Spatial correlations between the biphenyl cores of the system are impeded by the ordering or freezing of the aliphatic chains. The appearance of the scattering around 110 Å in the SAXS regime is concurrent with ordering of the system on the 3.8 Å length scale; therefore, in this framework, the smectic demixing of the system results in a mesogen-rich phase that crystallizes on formation and, as mentioned, is likely driven energetically by the enthalpy of this crystallization.

The mechanism proposed above is further supported by SAXS and WAXS data collected from a liquid crystalline diblock copolymer formed by the complexation of the imidazole mesogen with the PAA block of a poly(styrene-*b*-acrylic acid) backbone. Here crucial insight has been gained from magnetic field alignment of the material, which enables the resolution in SAXS of the orientation of the supramolecular structure at ~110 Å relative to the two smaller length scale LC structures. The data (Supporting Information: Figures S3 and S4) show that the large length scale structure and the smaller LC structures are collinear in their lattice vectors, consistent with the schematic representation of Figure 11b. In the wide-angle regime, the delineation

between the packing of biphenyl cores versus the alkyl constituents of the mesogens as a function of stoichiometry is particularly clear and shows that layer tilt is driven by crystallization of alkyl chains on the 3.8 Å length scale.

## Conclusions

The facile assembly of functional, stimuli-responsive materials via supramolecular engineering motivates continued study of the phase behavior of these systems. Here a detailed investigation of a model system has revealed an unexpected complexity in the phase behavior. The deviation from the characteristic 1-D swelling behavior, which is commonly observed in side-chain complexed polymers, is certainly intriguing and warrants further investigation. From our FTIR data, it is clear that the assumption that the polymer actively binds all available ligands at substoichiometric ratios does not apply in the present case. Rather, the polymer exhibits a limited capacity for the mesogenic ligand, with binding saturated for $S \geq 0.33$. Such a result can be rightly viewed in the context of the entropic penalty suffered by the polymer backbone on dense complexation by the bulky mesogen, which acts to stretch the polymer backbone. Similar chain stretching is encountered in molecular bottle brushes where wormlike as opposed to Gaussian conformations of a flexible polymer backbone arise because of a high grafting density of side chains.[44,45] In the case of hydrogen-bonded side chains or mesogens as considered here, the backbone may provide an entropic mechanism to limit the extent of binding thermodynamically. Regardless of the origin, this limited capacity of the polymer for the mesogen has important implications for the phase behavior of the system because it enables mesogens present beyond the saturation stoichiometry to act as a solvent for the polymer at elevated temperatures. This solvency appears to be key in the display of the supramolecular length scale structures observed for samples with $S \geq 0.50$ as a consequence of smectic demixing between ligand-rich and ligand-poor mesophases. We have presented strong evidence that this mode of phase separation is active in the currently discussed system and have proposed a model that captures the salient features of the experimental data. This proposed model provides a basis for future studies utilizing polymer backbones with controlled stoichiometries of covalently attached mesogens mixed with varying amounts of the free mesogen and examined as a function of temperature.

**Acknowledgment.** We are grateful to Prof. P. Van Tassel and Jennifer Phelps for invaluable assistance with FTIR measurements and Ajay Negi and Pawel Majewski for helping with the experimental setup. This work was supported by the NSF under DMR-0847534.

**Supporting Information Available:** Details of the synthetic method for the production of the mesogen, additional DSC data taken at high heating rate, and additional temperature-resolved SAXS measurements. This material is available free of charge via the Internet at http://pubs.acs.org.

## References and Notes

(1) Kawakami, T.; Kato, T. *Macromolecules* **1998**, *31*, 4475–4479.
(2) Ruokolainen, J.; ten Brinke, G.; Ikkala, O.; Torkkeli, M.; Serimaa, R. *Macromolecules* **1996**, *29*, 3409–3415.
(3) Ruokolainen, J.; Torkkeli, M.; Serimaa, R.; Vahvaselka, S.; Saariaho, M.; ten Brinke, G.; Ikkala, O. *Macromolecules* **1996**, *29*, 6621–6628.
(4) Ruokolainen, J.; Tanner, J.; Ikkala, O.; ten Brinke, G.; Thomas, E. L. *Macromolecules* **1998**, *31*, 3532–3536.
(5) Chen, H. L.; Hsiao, M. S. *Macromolecules* **1999**, *32*, 2967–2973.
(6) Kato, T.; Kihara, H.; Ujiie, S.; Uryu, T.; Frechet, J. M. J. *Macromolecules* **1996**, *29*, 8734–8739.
(7) Sijbesma, R. P.; Beijer, F. H.; Brunsveld, L.; Folmer, B. J. B.; Hirschberg, J.; Lange, R. F. M.; Lowe, J. K. L.; Meijer, E. W. *Science* **1997**, *278*, 1601–1604.
(8) Ikkala, O.; ten Brinke, G. *Chem. Commun.* **2004**, 2131–2137.
(9) Hammond, M. R.; Mezzenga, R. *Soft Matter* **2008**, *4*, 952–961.
(10) Kato, T.; Frechet, J. M. J. *Macromolecules* **1989**, *22*, 3818–3819.
(11) Kato, T.; Kihara, H.; Uryu, T.; Fujishima, A.; Frechet, J. M. J. *Macromolecules* **1992**, *25*, 6836–6841.
(12) Osuji, C.; Chao, C. Y.; Bita, I.; Ober, C. K.; Thomas, E. L. *Adv. Funct. Mater.* **2002**, *12*, 753–758.
(13) Valkama, S.; Kosonen, H.; Ruokolainen, J.; Haatainen, T.; Torkkeli, M.; Serimaa, R.; ten Brinke, G.; Ikkala, O. *Nat. Mater.* **2004**, *3*, 872–876.
(14) Kosonen, H.; Ruokolainen, J.; Knaapila, M.; Torkkeli, M.; Jokela, K.; Serimaa, R.; ten Brinke, G.; Bras, W.; Monkman, A. P.; Ikkala, O. *Macromolecules* **2000**, *33*, 8671–8675.
(15) Chao, C. Y.; Li, X. F.; Ober, C. K.; Osuji, C.; Thomas, E. L. *Adv. Funct. Mater.* **2004**, *14*, 364–370.
(16) Mao, G. P.; Wang, J. G.; Ober, C. K.; Brehmer, M.; O'Rourke, M. J.; Thomas, E. L. *Chem. Mater.* **1998**, *10*, 1538–1545.
(17) Naciri, J.; Pfeiffer, S.; Shashidhar, R. *Liq. Cryst.* **1991**, *10*, 585–591.
(18) Ruokolainen, J.; Torkkeli, M.; Serimaa, R.; Komanschek, B. E.; Ikkala, O.; ten Brinke, G. *Phys. Rev. E* **1996**, *54*, 6646–6649.
(19) Ruokolainen, J.; Torkkeli, M.; Serimaa, R.; Komanschek, E.; ten Brinke, G.; Ikkala, O. *Macromolecules* **1997**, *30*, 2002–2007.
(20) Akiba, I.; Akiyama, S. *Macromolecules* **1999**, *32*, 3741–3745.
(21) Ruokolainen, J.; Makinen, R.; Torkkeli, M.; Makela, T.; Serimaa, R.; ten Brinke, G.; Ikkala, O. *Science* **1998**, *280*, 557–560.
(22) Tanaka, F.; Ishida, M. *Macromolecules* **1997**, *30*, 1836–1844.
(23) Dormidontova, E.; ten Brinke, G. *Macromolecules* **1998**, *31*, 2649–2660.
(24) Tsao, C. S.; Chen, H. L. *Macromolecules* **2004**, *37*, 8984–8991.
(25) Ikkala, O.; Ruokolainen, J.; ten Brinke, G.; Torkkeli, M.; Serimaa, R. *Macromolecules* **1995**, *28*, 7088–7094.
(26) ten Brinke, G.; Ruokolainen, J.; Ikkala, O. In *Hydrogen Bonded Polymers*; Binder, W., Ed.; Advances in Polymer Science *207*; Springer: New York, 2007; pp 113−177.
(27) Tung, S. H.; Xu, T. *Macromolecules* **2009**, *42*, 5761–5765.
(28) Lee, J. Y.; Painter, P. C.; Coleman, M. M. *Macromolecules* **1988**, *21*, 954–960.
(29) High, M. S.; Painter, P. C.; Coleman, M. M. *Macromolecules* **1992**, *25*, 797–801.
(30) ElMiloudi, K.; Djadoun, S. *Macromol. Symp.* **2008**, *265*, 89–99.
(31) Coleman, M. M.; Painter, P. C. *Prog. Polym. Sci.* **1995**, *20*, 1–59.
(32) Chao, C. Y.; Li, X. F.; Ober, C. K. *Pure Appl. Chem.* **2004**, *76*, 1337–1343.
(33) Osuji, C. O.; Chao, C. Y.; Ober, C. K.; Thomas, E. L. *Macromolecules* **2006**, *39*, 3114–3117.
(34) Sigaud, G.; Achard, M. F.; Hardouin, F.; Coulon, C.; Richard, H.; Mauzac, M. *Macromolecules* **1990**, *23*, 5020–5024.
(35) Sigaud, G.; Achard, M. F.; Hardouin, F.; Mauzac, M.; Richard, H.; Gasparoux, H. *Macromolecules* **1987**, *20*, 578–585.
(36) Ringsdorf, H.; Schmidt, H. W.; Schneller, A. *Makromol. Chem., Rapid Commun.* **1982**, *3*, 745–751.
(37) Scruggs, N. R.; Kornfield, J. A. *Macromol. Chem. Phys.* **2007**, *208*, 2242–2253.
(38) Chiu, H. W.; Zhou, Z. L.; Kyu, T.; Cada, L. G.; Chien, L. C. *Macromolecules* **1996**, *29*, 1051–1058.
(39) Brochard, F.; Jouffroy, J.; Levinson, P. *J. Phys.* **1984**, *45*, 1125–1136.
(40) Casagrande, C.; Veyssie, M.; Finkelmann, H. *J. Phys., Lett.* **1982**, *43*, L671–L675.
(41) Kempe, M. D.; Kornfield, J. A.; Ober, C. K.; Smith, S. D. *Macromolecules* **2004**, *37*, 3569–3575.
(42) Kihara, H.; Kishi, R.; Miura, T.; Kato, T.; Ichijo, H. *Polymer* **2001**, *42*, 1177–1182.
(43) Laffitte, J. D.; Achard, M. F.; Hardouin, F.; Nguyen, H. T.; Sigaud, G. *Liq. Cryst.* **1994**, *17*, 487–498.
(44) Zhang, B.; Grohn, F.; Pedersen, J. S.; Fischer, K.; Schmidt, M. *Macromolecules* **2006**, *39*, 8440–8450.
(45) Sheiko, S. S.; Borisov, O. V.; Prokhorova, S. A.; Moller, M. *Eur. Phys. J. E* **2004**, *13*, 125–131.